The $[Mn_2(2\text{-}OHsalpn)_2]^{2-,-,0,+}$ System: Synthesis, Structure, Spectroscopy, and Magnetism of the First Structurally Characterized Dinuclear Manganese Series Containing Four Distinct Oxidation States

Andrew Gelasco,[†] Martin L. Kirk,[‡] Jeff W. Kampf,[†] and Vincent L. Pecoraro*[,†]

Departments of Chemistry, The University of Michigan, Ann Arbor, Michigan 48109-1055, and The University of New Mexico, Albuquerque, New Mexico 87131-1096

Received February 6, 1997[⊗]

The series of complexes $[Mn_2(2\text{-}OH(Xsal)pn)_2]^{2-,-,0,+}$ [where 2-OH(Xsal)pn represents substituted-phenyl-ring derivatives (X = H, 5-Cl, 3,5-Cl_2, 5-NO_2) of 1,3-bis(salicylideneamino)-2-propanol] allow for the first detailed structural, magnetic, and spectroscopic study of a series of complexes that are the most active functional models for the manganese catalases. Representative examples of each oxidation state of the series (mimicking all of the known oxidation states for the enzyme's reaction chemistry) have been crystallographically characterized. The molecules presented herein are described as symmetric derivatives because they form dimers with both of the ligands spanning both Mn ions with the alkoxide on the backbone of the ligand bridging the metals. The variation in Mn−Mn separation across the four structures is 0.11 Å [Mn(II)−Mn(II) = 3.33 Å; Mn(II)−Mn(III) = 3.25 Å; Mn(III)−Mn(III) = 3.36 Å; Mn(III)−Mn(IV) = 3.25 Å], showing that the basic core structure is highly invariant. Nonetheless, significant structural changes in the polyhedra of each manganese ion can be observed across the range of metal oxidation states. These symmetric structures are distinct from the previously described asymmetric $\{[Mn_2(2\text{-}OH(Xsal)pn)_2](sol)\}^{0,+}$ structures which have only one bridging alkoxide and one monodentate solvent bound to the Mn(III) ion. These two forms (symmetric and asymmetric) are reminiscent of the carboxylate shift in metal carboxylate chemistry and illustrate how alkoxide ligands can participitate in an analogous alkoxide shift in order to generate a binding site for an incoming ligand, such as methanol, or substrate, such as hydrogen peroxide. This is the first series that allows the observation of the effect of subtle changes in geometry on the sign if not the magnitude of magnetic exchange in dimeric systems across a range of oxidation states. Regardless of the symmetric or asymmetric nature of the complex, the exchange parameter *J* was found to be very low; however, both ferro- and antiferromagnetic exchange can be realized with these dimers.

Manganese plays an essential and versatile role in the biochemistry of many microorganisms, plants, and animals. There are numerous enzymes that exploit the redox capabilities of manganese, including the manganese superoxide dismutases, manganese peroxidases, the oxygen-evolving complex (OEC), and dinuclear manganese redox enzymes such as manganese ribonucleotide reductase and the manganese catalases.[1−3]

Manganese catalases use a dinuclear active site to catalyze the disproportionation of H_2O_2 to dioxygen and water. A low-resolution structure of the *Thermus thermophilus* enzyme demonstrates that two manganese ions are in close proximity (≈3.6 Å).[4,5] EPR spectroscopy confirms that the manganese ions are weakly exchange coupled in the Mn^{II}_2 and $Mn^{II}Mn^{III}$ forms and more strongly coupled in the $Mn^{III}Mn^{IV}$ enzyme.[6,7] Considering all of the manganese catalases together, there have been four cluster oxidation levels that are established: Mn^{II}_2, $Mn^{II}Mn^{III}$, Mn^{III}_2, and $Mn^{III}Mn^{IV}$. The as-isolated enzyme from *T. thermophilus* contains a mixture of these states. The Mn^{II}_2 enzyme can be prepared by the addition of hydroxylamine to the isolated enzyme. If hydrogen peroxide is added to this sample, without removing the hydroxylamine, the enzyme is converted to the $Mn^{III}Mn^{IV}$ form; however, if the hydroxylamine is first removed, the enzyme turns over normally between the Mn^{II}_2 and Mn^{III}_2 oxidation states and large amounts of the $Mn^{III}Mn^{IV}$ form are not detected.[8]

While many dinuclear manganese complexes have been prepared using a variety of ligands, very few examples exist of dimers that can be isolated in more than two stable oxidation states. An example of a system with three stable oxidation states was recently published by Holm and co-workers utilizing a pentadentate ligand containing three phenolate groups.[9,10] They were able to isolate a series of iron[9] and manganese complexes[10] with the range of oxidation states M^{II}_2, $M^{II}M^{III}$, and M^{III}_2. In addition, while many Mn^{II}, Mn^{III}, Mn^{IV}, and even Mn^{V} complexes have been reported, functional synthetic analogues have been rare.[11−18]

We have prepared numerous manganese complexes using the ligand 2-OH(Xsal)pn(1,3-bis(salicylideneamino)-2-propanol, struc-

[†] The University of Michigan.
[‡] The University of New Mexico.
[⊗] Abstract published in *Advance ACS Abstracts,* April 1, 1997.

(1) Pecoraro, V. L., Ed. *Manganese Redox Enzymes*; VCH Publishers, Inc.: New York, 1992; p 303.
(2) Debus, R. J. *Biochim. Biophys. Acta* **1992**, *1102,* 269.
(3) Pecoraro, V. L.; Gelasco, A.; Baldwin, M. J. In *Mechanistic Bioinorganic Chemistry*; Thorp, H. H., Pecoraro, V. L., Eds.; Advances in Chemistry Series 244; American Chemical Society: Washington, DC, 1995.
(4) Barynin, V. V.; Vagin, A. A.; Melik-Adamyan, V. R.; Grebenko, A. I.; Khangulov, S. V.; Popov, A. N.; Andrianova, M. E.; Vainshtein, B. K. *Dokl. Akad. Nauk SSSR* **1986**, *288,* 877−880.
(5) Barynin, V. V.; Grebenko, A. I. *Dokl. Akad. Nauk SSSR* **1986**, *286,* 461−464.
(6) Khangulov, S. V.; Voyevodskaya, N. V.; Barynin, V. V.; Grebenko, A. I.; Melik-Adamyan, V. R. *Biofizika* **1987**, *32,* 960−966.
(7) Fronko, R. M.; Penner-Hahn, J. E.; Bender, C. J. *J. Am. Chem. Soc.* **1988**, *110,* 7554−7555.
(8) Penner-Hahn, J. E. Structural Properties of the Manganese Site in the Manganese Catalases. In *Manganese Redox Enzymes*; Pecoraro, V. L., Ed.; VCH Publishers, Inc.: New York, 1992; pp 29−45.
(9) Snyder, B. S.; Patterson, G. S.; Abrahamson, A. J.; Holm, R. H. *J. Am. Chem. Soc.* **1989**, *111,* 5214−5223.
(10) Yu, S.-B.; Wang, C.-P.; Day, E. P.; Holm, R. H. *Inorg. Chem.* **1991**, *30.* 4067−4074.

S0020-1669(97)00140-7 CCC: $14.00

ture **I**). Included among the structure types were monomeric

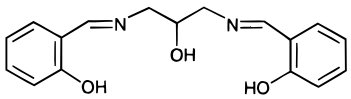

I

species,[19−21] infinite chains,[20] and monoalkoxo-bridged dimers.[20−23] More recently we presented a new structural class for dimers containing this ligand that contained two bridging alkoxides.[11] These complexes can be prepared by synthesis in nondonating solvents or, in some cases, by recrystallization of the asymmetric monoalkoxo-bridged dimers in acetonitrile or dichloromethane. We showed that the new geometry can have dramatic influences on the reactivity of these complexes with hydrogen peroxide. We now present a detailed structural, magnetic, and spectroscopic study of a series of complexes that are the first functional models for the manganese catalases that have been crystallographically characterized in all of the known oxidation states for the enzyme's reaction chemistry. In a separate paper, we will describe the functional hydrogen peroxide disproportionation chemistry exhibited by these molecules.[24]

Experimental Section

Materials. Salicylaldehyde and 2-hydroxy-5-nitrobenzaldehyde were used as received from Aldrich. 5-Chlorosalicylaldehyde and 3,5-dichlorosalicylaldehyde were obtained from TCI America. 1,3-Diaminopropan-2-ol was obtained from Fluka. Solvents were reagent grade from Mallinckrodt; electrochemical solvents were spectrochemical grade from Burdick and Jackson and were used without further purification. $(TBA)PF_6$ was prepared from ammonium hexafluorophosphate and tetrabutylammonium bromide and was recrystallized from ethanol. $NaClO_4$ was obtained from Aldrich and used without further purification. Thianthryl perchlorate was prepared by the reaction of thianthrene with concentrated perchloric acid in CH_2Cl_2 and was isolated as described.[25] (*Caution!* This compound has been reported to decompose explosively. It should be prepared in small quantities, and unused material should be destroyed by reaction with water after 5 days.)

Synthesis of the $[Mn_2(2\text{-}OHsalpn)_2]^{2-,-,0,+}$ Complexes. The ligands 2-OH(Xsal)pnH_3 (where X = 5-NO_2, 5-Cl, or 3,5-Cl_2) were prepared by the condensation of 2 equiv of the substituted salicylaldehyde with 1 equiv of 1,3-diaminopropan-2-ol, in methanol, and were isolated as crystalline solids.

(a) $(TEA)_2[Mn^{II}_2(2\text{-}OH(5\text{-}Cl\text{-}sal)pn)_2]$, 1. Three equivalents of (TEA)OH (30 mmol, 20 mL of a 1.5 M solution in methanol) was added to a slurry of 10 mmol of 2-OH(5-Cl-sal)pn (3.67 g) in 70 mL of methanol. The solvent was removed and the yellow oily residue redissolved in degassed acetonitrile. A solution of 10 mmol of $Mn(ClO_4)_2\cdot 6H_2O$ (3.62 g) in 10 mL of degassed acetonitrile was added to the ligand solution. The reaction mixture immediately turned a deep orange and was stirred for 1 h. The volume was reduced by half, leading to a microcrystalline orange solid that precipitated overnight. The orange product was collected under Ar and dried in vacuo for 4 h. Anal. Calcd for $Mn_2C_{54}H_{72}N_8O_6Cl_4$ (87% yield): C, 54.92; H, 6.15; N, 9.49; Mn, 9.30. Found: C, 54.86; H, 6.36; N, 9.32; Mn, 9.58.

(b) $(TMA)_2[Mn^{II}_2(2\text{-}OH(5\text{-}NO_2sal)pn)_2]\cdot 2DMF\cdot Et_2O$, 1a. Three equivalents of tetramethylammonium hydroxide (15 mmol, 6.25 mL of a 2.4 M solution in methanol) was added to a slurry of 5 mmol of 2-OH(5-NO_2sal)pn (1.94 g) in 100 mL of methanol. A solution of 5 mmol of $Mn^{II}(ClO_4)_2\cdot 6H_2O$ (1.81 g) in 10 mL of degassed methanol was added to the ligand solution. The reaction mixture immediately turned red-orange, and a red powder precipitated after 10 min of stirring. The powder was collected under Ar and dried in vacuo overnight. The complex was recrystallized from DMF/ether. Red crystals were obtained in 81% yield. Anal. Calcd for $Mn_2C_{52}H_{74}N_{12}O_{17}$: C, 49.05; H, 5.21; N, 13.98; Mn, 9.97. Found: C, 48.99; H, 5.25; N, 14.01; Mn, 10.0. Single crystals suitable for X-ray diffraction were grown under Ar by vapor phase diffusion of ether into a DMF solution of $(TMA)_2[Mn^{II}_2(2\text{-}OH(5\text{-}NO_2sal)pn)_2]$ at room temperature.

(c) $[Mn^{III}_2(2\text{-}OH(5\text{-}Cl\text{-}sal)pn)_2]$, 2. Method 1. $(TEA)_2[Mn^{II}_2(2\text{-}OH(5\text{-}Cl\text{-}sal)pn)_2]\cdot 2CH_3CN$, **1**$\cdot 2CH_3CN$ (1.0 mmol, 1.18 g), was dissolved in 300 mL of acetonitrile, and air was bubbled through the solution for 20 min, during which the solution changed color from orange-red to deep green-brown. After standing overnight, the mixture was filtered, and the filtrate was evaporated under a flow of N_2 until the volume was reduced to 100 mL. Brown blocklike crystals formed overnight at −20 °C, and analyzed as $[Mn^{III}_2(2\text{-}OH(5\text{-}Cl\text{-}sal)pn)_2]\cdot CH_3CN$ (94% yield). Anal. Calcd for $Mn_2C_{36}H_{29}N_5O_6Cl_4$: C, 49.17; H, 3.32; N, 7.96; Mn, 12.5. Found: C, 49.31; H, 3.35; N, 7.90; Mn, 12.4. These crystals were not suitable for X-ray diffraction.

Method 2. $[Mn^{III}_2(2\text{-}OH(5\text{-}Cl\text{-}sal)pn)_2(CH_3OH)]\cdot CH_3OH$, **5**, was prepared as previously described.[20] Green powdered **5** (1.0 g) was dissolved in 150 mL of acetonitrile, and the mixture was stirred for 1 h. The solvent was removed under reduced pressure, and the brown residue was redissolved in 300 mL of dry acetonitrile. Upon 2 days of standing at −20 °C, brown crystals were obtained from the solution. These crystals analyzed as $[Mn^{III}_2(2\text{-}OH(5\text{-}Cl\text{-}sal)pn)_2]\cdot CH_3CN$ (78% yield). Anal. Calcd for $Mn_2C_{36}N_5O_6Cl_4$: C, 49.17; H, 3.32; N, 7.96; Mn, 12.5. Found: C, 49.05; H, 3.30; N, 7.90; Mn, 12.5.

(d) $[Mn^{III}_2(2\text{-}OH(5\text{-}NO_2sal)pn)_2]$, 2a. The Na^+ salt of the 5-NO_2 derivative of **1** was prepared, by using the 5-NO_2-substituted ligand and NaOMe as the base. To a slurry of $Na_2[Mn^{II}(2\text{-}OH(5\text{-}NO_2sal)pn)]_2$, **1a**, in acetonitrile, was added 2.1 equiv of 15-crown-5. The solution was stirred for 10 min, at which point all of the Mn(II) complex had dissolved. Upon 2 days of standing in air, dark red blocklike crystals precipitated from the light red-orange solution. These crystals were used for crystallographic analysis.[11]

(e) $(TEA)[Mn^{II}Mn^{III}(2\text{-}OH(5\text{-}Cl\text{-}sal)pn)_2]$, 3. $(TEA)_2[Mn^{II}_2(2\text{-}OH(5\text{-}Cl\text{-}sal)pn)_2]\cdot 2CH_3CN$, **1**$\cdot 2CH_3CN$ (0.25 mmol, 0.295 g), was dissolved in 15 mL of warm (∼50 °C) degassed acetonitrile. A hot (65 °C) degassed acetonitrile solution of $[Mn^{III}_2(2\text{-}OH(5\text{-}Cl\text{-}sal)pn)_2]\cdot CH_3CN$, **2**$\cdot CH_3CN$ (0.25 mmol, 0.220 g) was added under Ar to this solution. The solution became red upon addition of the Mn^{III} complex, and a bronze-colored microcrystalline product precipitated upon cooling of the reaction mixture to room temperature (∼30 min). The product was collected under Ar and dried in vacuo for 2 h, yielding 0.330 g (68% yield) of **3**. Anal. Calcd for $Mn_2C_{42}H_{46}N_5O_6Cl_4$: C, 52.08; H, 4.79; N, 7.23; Mn, 11.34. Found: C, 51.65; H, 4.99; N, 7.01; Mn, 11.2.

Single crystals of $(TEA)[Mn^{II}Mn^{III}(2\text{-}OH(5\text{-}Cl\text{-}sal)pn)_2]\cdot C_6H_6\cdot CH_3OH$, **3a**, were prepared by mixing 40 mL of degassed benzene with 5 mL of a concentrated methanol solution of **3**. Dark orange crystals formed upon standing under Ar for 3 days.

(f) $[Mn^{III}Mn^{IV}(2\text{-}OH(3,5\text{-}Cl_2sal)pn)_2](ClO_4)$, 4. Method 1. $[Mn^{III}_2(2\text{-}OH(3,5\text{-}Cl_2sal)pn)_2]$ was prepared from the air oxidation of $Na_2[Mn^{II}_2(2\text{-}OH(3,5\text{-}Cl_2sal)pn)_2]$ in dichloromethane. The Mn^{III} dimer was isolated to give a brown microcrystalline solid. To a dry acetonitrile solution of $[Mn^{III}_2(2\text{-}OH(3,5\text{-}Cl_2sal)pn)_2]$ (0.1 mmol in 100 mL) was added thianthryl perchlorate (0.1 mmol in 200 mL of acetonitrile), and the

(11) Gelasco, A.; Pecoraro, V. L. *J. Am. Chem. Soc.* **1993**, *115*, 7928−7929.
(12) Mathur, P.; Crowder, M.; Dismukes, G. C. *J. Am. Chem. Soc.* **1987**, *109*, 5227−5233.
(13) Larson, E. J.; Pecoraro, V. L. *J. Am. Chem. Soc.* **1991**, *113*, 7809−7810.
(14) Bossek, U.; Saher, M., Weyhermüller, T.; Wieghardt, K. *J. Chem. Soc., Chem. Commun.* **1992**, 5492.
(15) Kitajima, N.; Osawa, M.; Tamura, N.; Moro-oka, Y.; Hirano, T.; Nagano, T. *Inorg. Chem.* **1993**, *32*, 1879−1880.
(16) Sakiyama, H.; Okawa, H.; Isobe, R. *J. Chem. Soc., Chem. Commun.* **1993**, 882−884.
(17) Pessiki, P. J.; Dismukes, G. C. *J. Am. Chem. Soc.* **1994**, *116*, 898−903.
(18) Pessiki, P. J.; Khangulov, S. V.; Ho, D. M.; Dismukes, G. C. *J. Am. Chem. Soc.* **1994**, *116*, 891−897.
(19) Bonadies, J. A.; Maroney, M. J.; Pecoraro, V. L. *Inorg. Chem.* **1989**, *28*, 2044−2051.
(20) Bonadies, J. A.; Kirk, M. L.; Lah, M. S.; Kessissoglou, D. P.; Hatfield, W. E.; Pecoraro, V. L. *Inorg. Chem.* **1989**, *28*, 2037−2044.
(21) Bertoncello, K.; Fallon, G. D.; Murray, K. S.; Tiekink, E. R. T. *Inorg. Chem.* **1991**, *30*, 3562−3568.
(22) Larson, E.; Haddy, A.; Kirk, M. L.; Sands, R. H.; Hatfield, W. E.; Pecoraro, V. L. *J. Am. Chem. Soc.* **1992**, *114*, 6263−6265.
(23) Mikuriya, M.; Yamoto, T.; Tokii, T. *Bull. Chem. Soc. Jpn.* **1992**, 1466−1468.
(24) Gelasco, A.; Pecoraro, V. L. Submitted to *J. Am. Chem. Soc.*
(25) Gans, P.; Buisson, G.; Duée, E.; Marchon, J.-C.; Erler, E. S.; Scholz, W. F.; Reed, C. A. *J. Am. Chem. Soc.* **1986**, *108*, 1223−1234.

Table 1. Summary of Crystallographic Data for **1a**, **2a**, **3a**, and **4a**

	1a	**2a**	**3a**	**4a**
formula	$Mn_2C_{52}H_{74}N_{12}O_{17}$	$Mn_2C_{34}H_{26}N_8O_{14}$	$Mn_2C_{50}H_{56}N_5O_7Cl_4$	$Mn_2C_{44.5}H_{34}N_4O_{10}Cl_9$
fw	1249.12	880.52	1090.73	1213.75
space group	$P2_1/n$ (No. 14)	$P2_1/n$ (No. 14)	*Pbca* (No. 61)	$P\bar{1}$ (No. 2)
a, Å	14.601(4)	10.562(2)	11.372(3)	15.365(6)
b, Å	27.270(6)	14.084(4)	22.240(5)	16.113(6)
c, Å	14.998(3)	12.656(3)	40.30(1)	19.995(5)
α, deg	90	90	90	88.65(3)
β, deg	91.68(2)	113.18(2)	90	89.31(3)
γ, deg	90	90	90	78.04(3)
V, Å^3	5969(2)	1730(2)	10193(5)	4840(3)
Z	4	2	8	2
ρ_{calc}, g/cm^3	1.21	1.68	1.55	1.67
ρ_{obs},[a] g/cm^3	1.23	1.69	1.52	1.65
T, K	115	145	291	145
μ, cm^{-1}	4.8	7.8	7.3	10.62
no. of reflns: unique/obsd	11 329/7597 $[F_o \geq 4\sigma(F)]$	3415/2770 $[F_o \geq 2\sigma(F)]$	6686/3901 $[F_o \geq 3\sigma(F)]$	17 112/8885 $[F_o \geq 4\sigma(F)]$
no. of params	672	307	525	1215 in 2 blocks
data/param ratio	11.0	9.0	7.4	7.3
GOF	1.80	1.02	1.73	1.38
R (R_w)	0.0756 (0.0795)	0.0591 (0.0603)	0.0893 (0.0793)	0.0777 (0.0734)

mixture was stirred for 1 h. The solvent volume was reduced to one-third, 100 mL of dichloromethane was added, and the solution was stored overnight at −20 °C. Dark brown microcrystals were recovered from this flask. These crystals analyzed satisfactorily as $[Mn^{III}Mn^{IV}(2\text{-}OH(3,5\text{-}Cl_2sal)pn)_2](ClO_4)\cdot 2CH_2Cl_2$, **4**$\cdot 2CH_2Cl_2$; however, they were not suitable for X-ray studies. Anal. Calcd for $Mn_2C_{38}H_{26}N_4O_{10}Cl_{13}$: C, 34.72; H, 2.10; N, 4.50; Mn, 8.82. Found: C, 34.45; H, 2.05; N, 4.49; Mn, 8.8.

Method 2. As described in an earlier report,[22] the highly asymmetric complex $[Mn^{III}Mn^{IV}(2\text{-}OH(3,5\text{-}Cl_2sal)pn)_2(THF)](ClO_4)$, **6**, can be obtained by bulk electrolysis of $[Mn^{III}_2(2\text{-}OH(3,5\text{-}Cl_2sal)pn)_2(CH_3OH)]$ in a 0.1 M $NaClO_4$ solution in acetonitrile at 900 mV vs SCE and recrystallization of the product by slow evaporation of a THF solution. Black needle-like crystals formed overnight at −20 °C after the bulk electrolysis solution was evaporated to half of its original volume under N_2. These crystals analyze as $[Mn^{III}Mn^{IV}(2\text{-}OH(3,5\text{-}Cl_2sal)pn)_2](ClO_4)\cdot H_2O$. Anal. Calcd for $Mn_2C_{34}H_{24}N_4O_{11}Cl_9$: C, 37.34; H, 2.21; N, 5.12; Mn, 10.05. Found: C, 37.30; H, 2.21; N, 5.20; Mn, 9.94. The water is present only as a water of crystallization and does not cause the conversion to the asymmetric form of the complex.[26] If these crystals are dissolved in a 1:1 acetonitrile/toluene solution, black blocklike crystals of a toluene adduct form upon slow evaporation of the acetonitrile. These crystals are suitable for X-ray diffraction.

Instrumentation and Physical Methods. (a) IR and UV−Vis Spectroscopies. IR samples (4000−400 cm^{-1}) were prepared in KBr and run on a Nicolet FTIR. UV−vis spectra were taken in either acetonitrile or dichloromethane from 200 (230 in CH_2Cl_2) to 1600 nm on a Perkin-Elmer Lambda 9 UV−vis−near-IR spectrophotometer equipped with a PE 3600 data station.

(b) Electrochemistry. Cyclic voltammetry and bulk electrolysis studies were performed on a Bioanalytical Systems BAS-100 electrochemical analyzer. CV analysis was performed using a Pt disk working electrode, a Pt wire auxiliary electrode, and an SCE reference electrode, in acetonitrile with $(TBA)PF_6$ as the supporting electrolyte.

(c) EPR Spectroscopy. X-Band EPR spectra were collected by using a Bruker E100 spectrometer with a modified console. Spectra were obtained in the range 4.4−77 K with an Oxford Instruments ESR-900 continuous-flow cryostat. Spectra at 77 K were collected using a quartz liquid-N_2 finger Dewar insert.

(d) Magnetic Susceptibility Studies. Variable-temperature magnetic susceptibility data were collected between 2 and 300 K using a Quantum Design superconducting quantum interference device (SQUID) in an applied magnetic field of 5000 G. Variable-field magnetization data were collected at 2, 3.3, 5, and 10 K in applied magnetic fields up to 52 000 G. The magnetometer was calibrated with mercury tetrakis-(thiocyanato)cobaltate(II) as a standard. Diamagnetic corrections were made using Pascal's constants.[27−29] The powdered samples were contained in the small half of a gelatin capsule and prevented from torquing in the applied field by placing the inverted larger half of the gelatin capsule into the smaller half. The gelatin capsule sample holder assembly was then mounted in a clear soda straw which was fixed to the magnetometer drive rod.

X-ray Crystallographic Analysis. All crystals, sealed in capillary tubes, were mounted on the goniometer head of a Nicolet R3 four-circle diffractometer equipped with a low-temperature device, except for **3a**, which was mounted on a Syntex $P2_1$ diffractometer at room temperature. Intensity data were obtained by using Mo Kα radiation (0.7107 Å) monochromatized from a graphite crystal whose diffraction vector was parallel to the diffraction vector of the sample. Three standard reflections were measured every 97 reflections and were used for scaling the data in the case of decay (**3a**). Lattice parameters were determined from a least-squares refinement of 15−18 centered reflections obtained from rotation photographs. The data were reduced using the programs of the SHELXTL PLUS software set (Siemens Analytical X-Ray Instruments, Inc.) running on a Digital Equipment Corp. VAXStation 3500 computer. The structures were solved by direct methods, and in subsequent refinement the function $\sum w(|F_o| - |F_c|)^2$ was minimized where F_o and F_c are the observed and calculated structure factor amplitudes. The agreement indices $R = \sum||F_o| - |F_c||/|F_o|$ and $R_w = [\sum w(|F_o| - |F_c|)^2/\sum w|F_o|^2]^{1/2}$ were used to evaluate the results. Atomic scattering factors were taken from the *International Tables for X-ray Crystallography*. Hydrogen atoms were located or placed at 0.96 Å but not refined and were given fixed *U* values (isotropic temperature factors) of 0.08 Å^2, except for those of **2a**, whose structure was reported previously.[11] Fractional atomic coordinates, anisotropic thermal parameters, and complete bond lengths and angles of all non-hydrogen atoms for **1a**, **3a**, and **4a** are deposited as Supporting Information (Tables S1−S18). Table 1 contains a summary of data collection details and results for all four structures, and Table 2 contains selected bond angles for the four complexes. The $Mn_2N_4O_6$ cores of all four molecules are illustrated in Figure 1.

Results

Description of Structures. (a) $(TMA)_2[Mn^{II}(2\text{-}OH(5\text{-}NO_2\text{-}sal)pn)]_2\cdot 2DMF\cdot Et_2O$, 1a. The ORTEP diagram of the anion $[Mn^{II}(2\text{-}OH(5\text{-}NO_2sal)pn)]_2^{2-}$ is shown in Figure S1 (Supporting Information). All non-hydrogen atoms in the anion and the two tetramethylammonium cations were refined anisotropically. One DMF molecule was well-behaved, giving good distances, angles, and isotropic thermal parameters. The second DMF molecule

(26) Riggs-Gelasco, P. J.; Gelasco, A.; Wright, D.; Kitajima, N.; Armstrong, W. H.; Pecoraro, V. L.; Penner-Hahn, J. E. Manuscript in preparation.

(27) Figgis, B. N.; Lewis, J. In *Modern Coordination Chemistry*; Lewis, J., Wilkins, R. G., Eds. Interscience: New York, 1960; p 403.

(28) Konig, E. *Magnetic Properties of Transition Metal Compounds*; Springer-Verlag: Berlin, 1966.

(29) Weller, R. R.; Hatfield, W. E. *J. Chem. Educ.* **1979**, *56*, 652.

Table 2. Selected Bond Angles (deg) for **1a**, **2a**, **3a**, and **4a**[a]

	1a	2a	3a	4a
Mn1−O2−Mn2	101.3(1)	99.1(1)	103.9(3)	102.4(3)
Mn1−O5−Mn2	101.4(1)		103.8(3)	105.3(3)
O1−Mn1−O2	156.0(2)	87.8(1)	158.3(3)	170.5(3)
O1−Mn1−O5 [O2A]	102.7(2)	163.0(1)	97.4(3)	91.5(3)
O1−Mn1−O6 [O3]	86.8(2)	105.7(1)	89.8(3)	96.1(3)
O1−Mn1−N1	81.0(2)	89.1(1)	80.3(3)	89.1(3)
O1−Mn1−N4 [N3]	90.4(2)	93.2(1)	85.3(3)	89.2(3)
O2−Mn1−O5 [O2A]	79.3(2)	80.9(1)	83.3(3)	83.9(3)
O2−Mn1−O6 [O3]	101.8(2)	154.4(1)	93.7(3)	89.7(3)
O2−Mn1−N1	75.9(2)	108.2(1)	78.4(3)	82.8(3)
O2−Mn1−N4 [N3]	113.0(2)	72.7(1)	116.1(3)	98.3(3)
O2−Mn2−O3	140.1(2)		136.2(3)	148.1(3)
O2−Mn2−O4	96.2(2)		101.6(3)	84.6(3)
O2−Mn2−O5	78.0(2)		68.7(2)	68.4(3)
O2−Mn2−N2	74.8(2)		74.8(3)	75.2(3)
O2−Mn2−N3	127.1(2)		121.4(3)	111.5(3)
Mn···Mn, Å	3.332(6)	3.247(6)	3.360(7)	3.254(6)

[a] Atom designations in brackets correspond to **2a**. Important bond distances for each dimer are shown in Figure 1.

exhibited high thermal motion, indicating that there was some disorder in the molecule; in addition, some of the C−N bonds exhibited nonideal distances (*vide infra*). The diethyl ether, while having high isotropic thermal motion, exhibited good distances and angles and was modeled by the use of additional observational equations[30] and further refined as a rigid group. The second DMF was modeled as two partial molecules disordered between two positions around the N and carbonyl carbon (refined SOF = 0.61 and 0.39) by the addition of observational equations, fixing bond lengths for the molecule. The residual electron density corresponded to 1.3 e/Å^3, and the highest peaks were found near the disordered solvent molecules.

(b) [Mn^{III}(2-OH(5-NO$_2$sal)pn)]$_2$, 2a. The structure of **2a** was reported by us previously,[11] and subsequently the 3-NO$_2$ derivative, which is isostructural, appeared.[31] The asymmetric unit contains half of the complex with no solvent molecules. Figure S2 (Supporting Information) shows the ORTEP diagram of the complex with the heteroatoms labeled. The $Mn_2N_4O_6$ core is shown in Figure 1 for comparison to the other structures.

(c) (TEA)[Mn^{II}Mn^{III}(2-OH(5-Cl-sal)pn)$_2$]·C$_6$H$_6$·CH$_3$OH, 3a. The crystal was mounted with a drop of the mother liquor in the capillary, but still suffered from 35% decay over the course of data collection. The data were scaled by normalizing the check reflections. All non-hydrogen atoms of the anion and the tetraethylammonium cation were refined anisotropically. The benzene was refined as a rigid group with hydrogen atoms placed in idealized positions. The methanol molecule was modeled as two partial methyl groups disordered around a common oxygen atom. Figure 2 shows the ORTEP diagram of the anionic dimer. Figure 1 shows the $Mn_2N_4O_6$ core, and the full ORTEP with the complete numbering scheme for the anion is given as Figure S3 (Supporting Information).

(d) [Mn^{III}Mn^{IV}(2-OH(3,5-Cl$_2$sal)pn)$_2$](ClO$_4$)·1.5C$_7$H$_8$, 4a. The asymmetric unit consists of two different dimers, two perchlorate anions, and three toluene molecules. Reported distances and angles are for one of the dimers; however, the bond distances and angles for the other molecule are very similar. All parameters for both molecules are supplied in the Supporting Information. All non-hydrogen atoms in the cations were refined anisotropically, as well as the perchlorate Cl atoms. One of the three toluene molecules was disordered with respect to the methyl carbon placement but was modeled successfully. Figure 1 shows the $Mn_2N_2O_4$ core of the cation of dimer 1. ORTEP diagrams with the complete numbering schemes for each cation are supplied as Figures S4 and S5 (Supporting Information).

Electronic Spectra of Complexes. UV−vis spectra of the representative series of 2-OH(5-Cl-sal)pn dimers were collected from 200 to 1600 nm in acetonitrile. The spectra from 300 to 600 nm are shown in Figure 3. The mixed-valent dimer [Mn^{II}Mn^{III}(2-OH(5-Cl-sal)pn)$_2$]$^-$ exhibits a weak transition at 1200 nm (ϵ = 145 cm^{-1}·M^{-1}), consistent with an intervalence charge transfer band that is indicative of a dimer with a Robin and Day classification II exchange system.[32] This spectrum is shown as the inset in Figure S6 (Supporting Information). All of the dimer systems exhibit a similar systematic shift of the 380 nm band to lower energy upon sequential oxidation.

Electrochemistry. Cyclic voltammetry of Na$_2$[Mn^{II}(2-OH(5-NO$_2$sal)pn)]$_2$ (shown in Figure 4) indicates that oxidations to Mn^{II}Mn^{III}, Mn$^{III}_2$, and Mn^{III}Mn^{IV} are possible. Two of those oxidations are reversible. The average difference in the III/IV ↔ III$_2$ couple for all ring substituted derivatives is 575 ± 10 mV. The Mn^{II}Mn^{III} ↔ Mn$^{II}_2$ couple is nonreversible, and this behavior appears to be independent of ligand derivative or initial oxidation state. However, in the 5-NO$_2$ case, a pseudoreversible wave can be observed at −390 mV, which is 500 mV more negative than the III$_2$ ↔ II/III couple. On the basis of these data, an estimate for the Mn$^{III}_2$ ↔ Mn$^{II}_2$ couple can be made by assuming that the II/III ↔ II/II couple is 500 mV more negative than the III/III ↔ II/III couple for the appropriate ring-substituted derivative. Table 3 shows the relative III/IV ↔ III/III and III/III ↔ II/III and estimated III/III ↔ II/II redox couples for the substituted-ring series of symmetric dimers in acetonitrile.

EPR Spectra of Complexes. Three of the four oxidation states obtainable by these dimers are potentially EPR active at X-band frequencies. Figure 5A shows the EPR spectrum of a Mn$^{II}_2$ dimer at 5 K. The spectrum of Na$_2$[Mn^{II}(2-OH(5-NO$_2$sal)pn)]$_2$ in DMF is typical for weakly exchange-coupled Mn^{II} dimers.[12,33]

The one-electron-oxidized dimer exhibits an EPR spectrum at 77 K that is similar to spectra that have been observed for other characterized Mn^{II}Mn^{III} dimers.[34] These spectra are characterized by an absorptive feature at approximately $g = 7$ and lack any significant feature at $g = 2$. When the temperature is lowered to 5 K, the spectrum of [Mn^{II}Mn^{III}(2-OH(5-Clsal)-pn)$_2$]$^-$ does not change to a prominent $g = 2$ multiline signal but instead retains the low-field component as shown as Figure 5B. We assign this feature to the $S = {}^9/_2$ ground state predicted from the solid state magnetic studies (*vide infra*).

The most oxidized species of this series, [Mn^{III}Mn^{IV}(2-OH(3,5-Cl$_2$sal)pn)$_2$]$^+$, exhibits EPR signals in 50:50 butyronitrile/propionitrile (Figure 5C,D) that are very similar to those observed for the asymmetric monoalkoxo-bridge derivative [Mn^{III}Mn^{IV}(2-OH(3,5-Cl$_2$sal)pn)$_2$(DMF)]$^+$, **6**·DMF, in DMF.[22] Both species exhibit prominent absorptive features at $g = 5$ at 77 K, which are in thermal equilibrium with a 12-line "multiline" at $g = 2$ that can be observed upon lowering the temperature. While the main features of the spectra are similar between the two complexes, the interchange of the $g = 2$ and $g = 5$ signals shows a temperature dependence which is somewhat different for the dialkoxo-bridged derivative than for **6**. This is consistent with the difference in exchange coupling observed between the two complexes **4** and **6**.

(30) Waser, J. *Acta Crystallogr*. **1963**, *16*, 1091.
(31) Zhang, Z.-Y.; Brouca-Cabarrecq, C.; Hemmert, C.; Dahan, F.; Tuchagues, J.-P. *J. Chem. Soc., Dalton Trans*. **1995**, 1453−1460.
(32) Robin, M. B.; Day, P. *Adv. Inorg. Chem. Radiochem*. **1967**, *10*, 248.
(33) Mathur, P.; Dismukes, G. C. *J. Am. Chem. Soc*. **1983**, *105*, 7093−7098.
(34) Schake, A. R.; Schmitt, E. A.; Conti, A. J.; Streib, W. E.; Huffman, J. C.; Hendrickson, D. N.; Christou, G. *Inorg. Chem*. **1991**, *30*, 3192−3199.

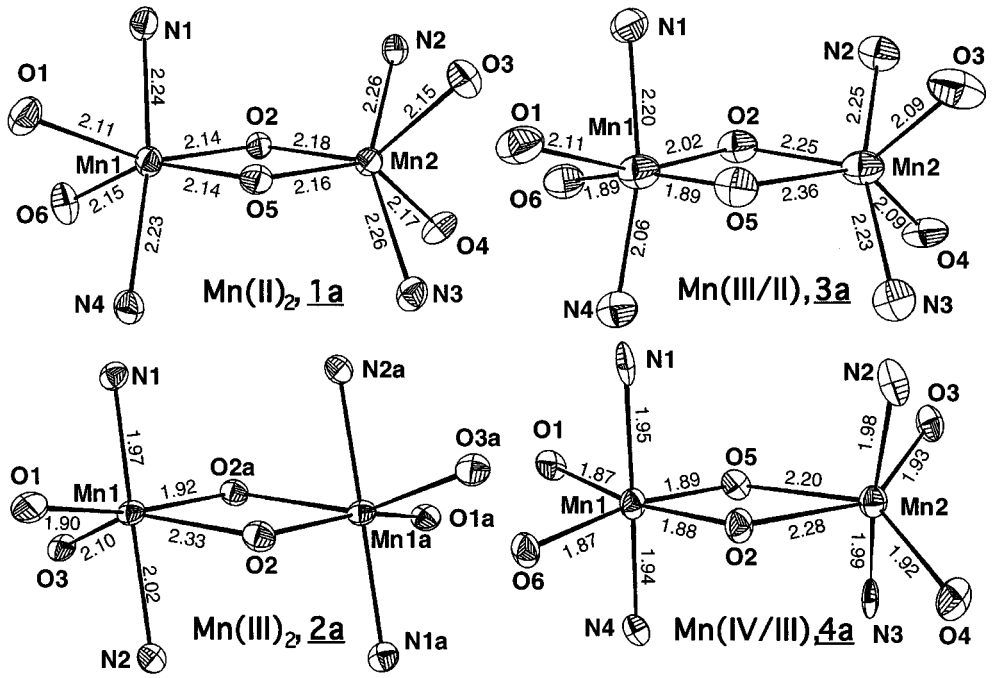

Figure 1. ORTEP structures for the metal−ligand environment of the four dimers. Important bond lengths are included for each dimer; bond angles are given in Table 2.

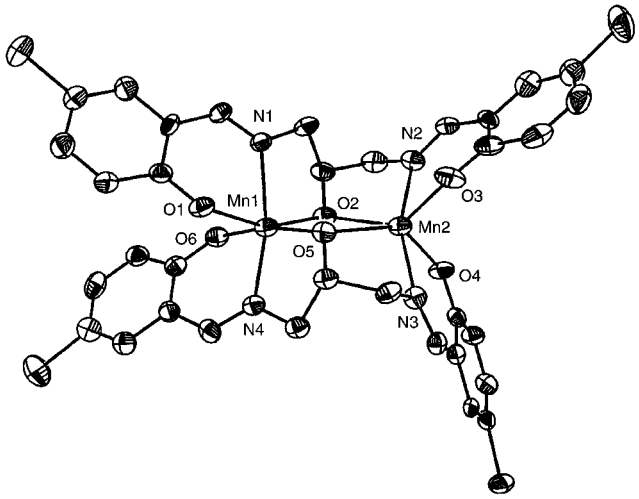

Figure 2. ORTEP diagram of the anion of (TEA)$[Mn_2(2\text{-}OH(5\text{-}Clsal)pn)_2]\cdot C_6H_6\cdot CH_3OH$, **3a**. Ellipsoids are shown at the 30% probability level.

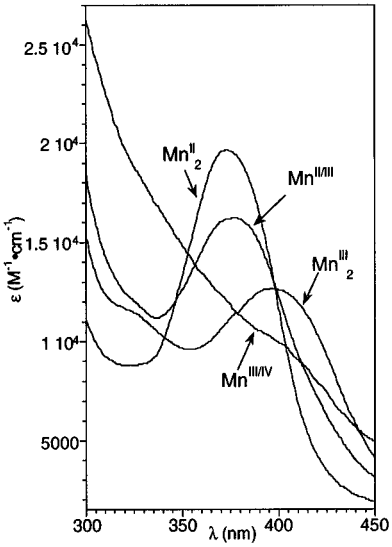

Figure 3. Electronic spectra of the $[Mn(2\text{-}OH(5\text{-}Clsal)pn)]_2$ dimers.

Magnetic Properties of Dimers. Variable-temperature magnetic susceptibility data were collected for all four oxidation states of the dimer series in the temperature range 2−300 K in a small applied field of 5000 G to minimize contributions from **g**-tensor anisotropy. Fits of the data to a model incorporating the single-ion zero-field splitting, *D*, the exchange interaction, *J*, the primary components of the **g** tensor (g_x, g_y, g_z), impurity corrections, and intercluster exchange interactions were not attempted in order to minimize effects of overparameterization. We chose to use a simple "exchange-only" model in order to assess the relative sign and magnitude of the exchange interactions in this dimer series and relate these parameters to differences in geometric and electronic structures. The Hamiltonian used in the analysis of the data is given in eq 1.

$$\mathbf{H} = g\beta H\cdot(S_1 + S_2) - 2J(S_1\cdot S_2) \qquad (1)$$

The Zeeman part of the Hamiltonian assumes that the *g* values for the two ions which comprise the dimer are isotropic and equivalent. The magnetic susceptibility data for each dimer were fit to the expression

$$\chi_m = \frac{Ng^2\beta^2}{kT}\sum_i \left[\frac{^1/_3 S_i(S_i+1)(2S_i+1)\exp(-E_i/kT)}{(2S_i+1)\exp(-E_i/kT)}\right] \qquad (2)$$

The E_i are the zero-field intradimer exchange energies given by

$$E_i = -J[S_i(S_i+1) - S_1(S_1+1) - S_2(S_2+1)] \qquad (3)$$

where S_1 and S_2 are the individual spins associated with the two Mn ions in the dimer and S_i assumes values $S_i = S_1 + S_2 + ... + |S_1 - S_2|$.

Figure 6 shows fits to the data for each dimer based on eq 2 for χ_m and for μ_{eff}, where μ_{eff} is given by eq 4.

$$\mu_{eff} = 2.83(\chi T)^{1/2} \qquad (4)$$

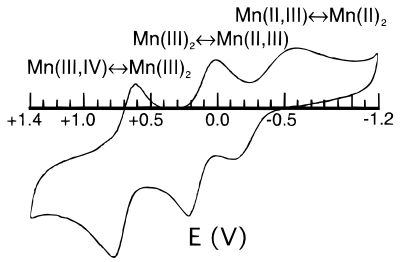

Figure 4. Cyclic voltammogram of $(TMA)_2[Mn^{II}_2(2\text{-}OH(5\text{-}NO_2sal)pn)_2]$ in acetonitrile. $E_{1/2}$ values of redox couples for this and other derivatives are compiled in Table 3.

Table 3. Redox Potentials of the Substituted-Ring Mn 2-OHsalpn Dimers

ring substitution	$E_{1/2}$(III$_2$ ↔ II/III), mV[a]	$E_{1/2}$(III/IV ↔ III$_2$), mV[a]	est $E_{1/2}$(III$_2$ ↔ II$_2$), mV[b]	ref
5-MeO	−368	202	−618	
H	−250	325	−500	
5-Cl	−148	435	−400	
3,5-Cl$_2$	−24	547	−270	
5-NO$_2$	113	695	−140 ± 30	
3-NO$_2$[c]	37	592	n/a	31

[a] All potentials are reported vs SCE and standardized vs ferrocene in acetonitrile. [b] Estimated redox potential for III$_2$ ↔ II$_2$ is based on Δ_{av}(III/IV ↔ III/II) = 575 mV; see Results for the method of calculation. [c] Values are given vs SCE in DMF solution.

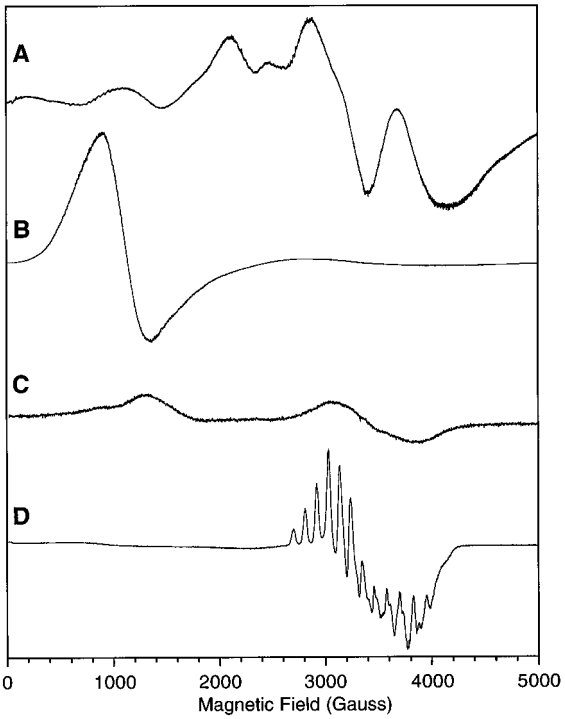

Figure 5. (A) EPR spectrum of $Na_2[Mn^{II}_2(2\text{-}OH(5\text{-}NO_2sal)pn)_2]$ at 5 K in DMF, 4.3 mM in dimer. (B) EPR spectrum of $TEA[Mn^{II}_2(2\text{-}OH(5\text{-}Cl\text{-}sal)pn)_2]$ at 5 K in ethanol. (C) 93 K and (D) 5 K EPR spectra of $[Mn^{III}Mn^{IV}(2\text{-}OH(3,5\text{-}Cl_2sal)pn)_2](ClO_4)$ in butyronitrile/propionitrile.

The susceptibility data for $(TMA)_2[Mn^{II}_2(2\text{-}OH(5\text{-}NO_2sal)pn)_2]$ and $(TEA)[Mn^{II}Mn^{III}(2\text{-}OH(5\text{-}Cl\text{-}sal)pn)_2]$ are shown in Figure 6A,B. Both complexes display an increase in μ_{eff} with decreasing temperature, which clearly indicates that these compounds are ferromagnetically exchange coupled and possess ground spin states of $S = 5$ and $S = {}^9/_2$, respectively. The dimer $(TMA)_2[Mn^{II}_2(2\text{-}OH(5\text{-}NO_2sal)pn)_2]$ is only the second example of a structurally characterized Mn^{II} dimer that is ferromagnetically coupled in the solid state.[35] Similarly, $(TEA)[Mn^{II}Mn^{III}(2\text{-}OH(5\text{-}Cl\text{-}sal)pn)_2]$ is only the second structurally characterized $Mn^{II}Mn^{III}$ complex to exhibit ferromagnetic coupling, the first being a phenolate-bridged compound prepared by Christou and co-workers.[34]

The susceptibility data for the higher valent complexes $[Mn^{III}(2\text{-}OH(5\text{-}Cl\text{-}sal)pn)]_2$, **2**, and $[Mn^{III}Mn^{IV}(2\text{-}OH(3,5\text{-}Cl_2sal)pn)_2]ClO_4$, **4**, are shown in Figure 6C,D. A recent study[31] of the magnetic behavior of the 3-NO_2 isomer of the $[Mn^{III}(2\text{-}OH(5\text{-}Cl\text{-}sal)pn)]_2$ dimer, **7**, included fitting the data to a zero-field-splitting parameter and an impurity correction that gave a similar result, which is included in Table 4. The magnetic susceptibility of $[Mn^{III}(2\text{-}OH(5\text{-}Cl\text{-}sal)pn)]_2$ turns over at ~30 K in a manner indicative of antiferromagnetic exchange coupling between the two Mn^{III} ions leading to an $S = 0$ ground state. The magnetic susceptibility data for $[Mn^{III}Mn^{IV}(2\text{-}OH(3,5\text{-}Cl_2sal)pn)_2]ClO_4$ indicate the presence of a paramagnetic ground state. However, the decrease in μ_{eff} with decreasing temperature provided strong evidence of intradimer antiferromagnetic exchange interactions yielding a ground spin state of $S = {}^1/_2$ for the complex. This compound, while dramatically different in structure, has solid state magnetic susceptibility behavior similar to that of $[Mn^{III}Mn^{IV}(2\text{-}OH(3,5\text{-}Cl_2sal)pn)_2(THF)]ClO_4$, **6**.[22] However, despite the fact that the Mn−Mn separation is ~0.3 Å shorter in **4**, the antiferromagnetic exchange between the Mn ions for **4** is even smaller than that in the asymmetrically bridged complex.

Discussion

Many dinuclear complexes of manganese having oxidation states from Mn^{II} to Mn^{IV} have been prepared; however, single-ligand systems with the ability to support more than two oxidation states are rare.[10] We were able to prepare a series of complexes containing the ligand 2-OHsalpn spanning the range from Mn^{II}_2 to $Mn^{III}Mn^{IV}$. This ligand gives us the range of oxidation states necessary for catalysis of hydrogen peroxide disproportionation and has the same air-stable oxidation state as the manganese catalases.[11,24] The ligand may also provide an internal mechanism for protonation and deprotonation of substrate and product while maintaining the dinuclear manganese active site through the dinucleating ligand.[24] An interesting feature of this series is the small span of Mn···Mn distances, 3.36−3.24 Å, observed across the four oxidation states.

Previous studies examined two of the oxidation states (Mn^{III}_2 and $Mn^{III}Mn^{IV}$) possible for asymmetric dimers[36] utilizing 2-OHsalpn.[20−23] By forcing both backbone alkoxides to bridge both Mn ions, we have been able to examine the effect of oxidation on a dinuclear series with invariant ligand sets across a much greater oxidation state range. We have found that the solution speciation (between symmetric and asymmetric derivatives) can be controlled by limiting the amount of donating solvent present in the solution. Thus, while solvents were not rigorously dried to remove water, the symmetric Mn^{III}_2 or $Mn^{III}Mn^{IV}$ dimers can be isolated if the concentration of water (or methanol) does not exceed 5% in acetonitrile solutions.[37] We have not found conditions where the Mn^{II}_2 or $Mn^{II}Mn^{III}$ dimers will bind solvent to form the asymmetric species.

Structures. All of the complexes have the ligand spanning both Mn ions with the alkoxide on the backbone of the ligand bridging the metals. The phenolate oxygen, imine nitrogen, and alkoxide oxygen form a meridional geometry around each Mn.

The Mn^{II}_2 derivative $(TMA)_2[Mn^{II}(2\text{-}OH(5\text{-}NO_2sal)pn)]_2\cdot 2DMF\cdot Et_2O$, **1a**, has two Mn^{II} ions in similar but not identical environments. One of the manganese ions is nearly a regular octahedron. The difference in the geometry between the two

(35) Cortés, R.; Pizarro, J. L.; Lazama, L.; Arriortua, M. I.; Rojo, T. *Inorg. Chem.* **1994**, *33*, 2697−2700.
(36) The monoalkoxide-bridged complexes are referred to as the asymmetric dimers, and the dialkoxide-bridged systems, as the symmetric dimers.
(37) Randall, D. E.; Gelasco, A.; Pecoraro, V. L.; Britt, R. D. *J. Am. Chem. Soc*, in press.

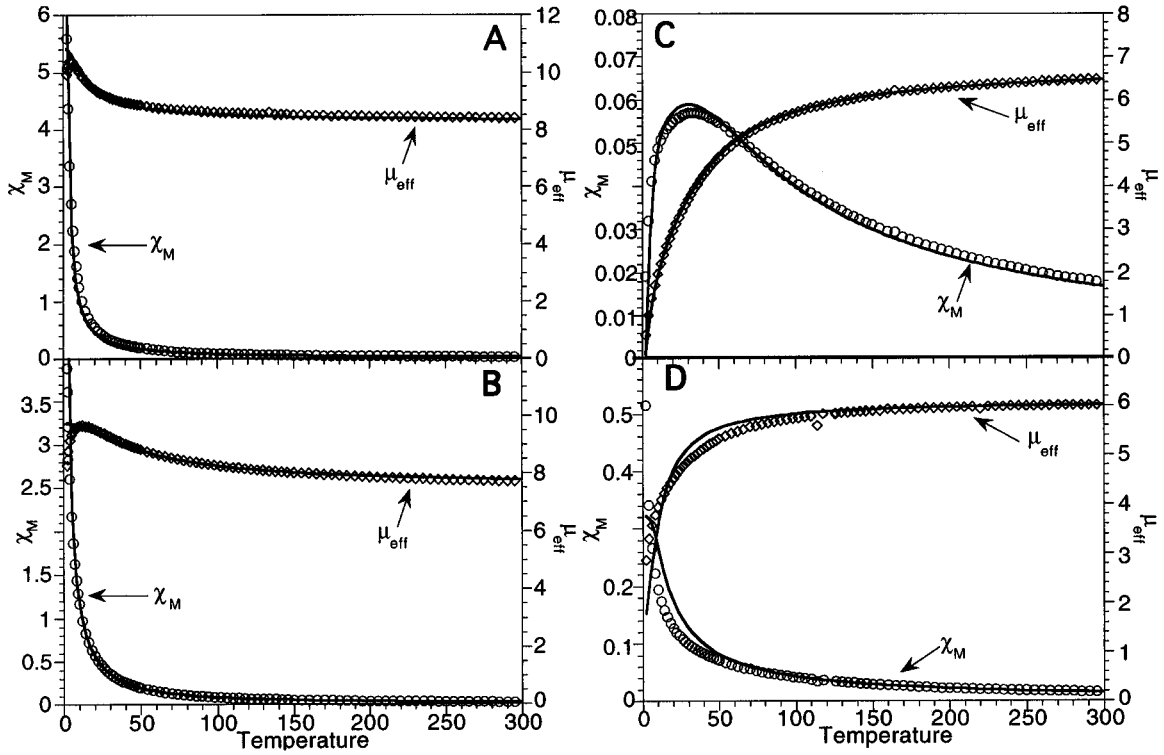

Figure 6. Plots of χ_M vs T and μ_{eff} vs T for (A) $(TMA)_2[Mn^{II}_2(2\text{-}OH(5\text{-}NO_2sal)pn)_2]$, **1a**, (B) $(TEA)[Mn^{II}Mn^{III}(2\text{-}OH(5\text{-}Clsal)pn)_2]$, **3**, (C) $[Mn^{III}_2(2\text{-}OH(5\text{-}Clsal)pn)_2]$, **2**, and (D) $[Mn^{III}Mn^{IV}(2\text{-}OH(3,5\text{-}Clsal)pn)_2](ClO_4)$, **4**. Best fit lines shown were calculated using eq 2, and relevant parameters are given in Table 4.

Table 4. Magnetic Parameters of Mn 2-OHsalpn Dimers

complex	J, cm^{-1}	g	P, Å	μ_{eff}, μ_B (room temp)[a]	ref
1a	0.52	1.97	2.15	8.42 (5.95)	
2·CH_3CN	−5.0	1.95	2.13	6.49 (4.59)	
3	3.23	1.93	2.13	7.72 (5.45)	
4	−2.0	1.95	2.07	6.04 (4.27)	
5	−3.55			6.86 (4.85)	20
6	−10	1.95		not reported	22
7	−1.62	2	2.13	7.03 (4.99)	31

[a] Values are per dimer. Values in parentheses are per Mn.

ions can be seen in the lengthening of the metal−ligand bonds around Mn2. Figure 1 shows the metal−ligand bond lengths for each dimer. The manganese−oxygen bonds are similar and the axial nitrogen−manganese bonds are longer by almost 0.1 Å for both ions. This is common for mixed oxygen−nitrogen ligand systems. The different coordination spheres for the Mn ions are probably a result of the strain on the Schiff base ligand imposed by the large ionic radius of Mn^{II}. This has been observed for other ligand systems[9,10] and is also seen for the Mn^{II} ion in the mixed-valent dimer $[Mn^{II}Mn^{III}(2\text{-}OH(5\text{-}Cl\text{-}sal)pn)_2]^-$.

The mixed-valent dimer $[Mn^{II}Mn^{III}(2\text{-}OH(5\text{-}Cl\text{-}sal)pn)_2]^-$ contains two valence-localized Mn ions. The Mn^{III} ion (Mn1, Figure 1 and Figure 2) has a characteristic tetragonal Jahn−Teller distortion. The axis formed by O5−Mn1-O6 is compressed, with a concomitant equatorial elongation of the other metal−ligand bonds. The effect of this distortion can be observed in the Mn^{II}−ligand bonds. The two bridging alkoxides in the Mn^{II}_2 dimer have identical bond lengths, whereas in the case of the $Mn^{II}Mn^{III}$ dimer, the Mn^{II}−alkoxide bond lengths differ by 0.13 Å. The Mn2−O5 bond length is very long (2.359 Å), and this lengthening is related to the contraction of the Mn1−O5 bond. The overall geometry of the ligand environment of the Mn^{II} ion (Mn2) is similar to that seen for Mn2 in **1a**. Interestingly this dimer has the longest Mn···Mn distance observed for this series, 3.36 Å.

The dimer $[Mn^{III}(2\text{-}OH(5\text{-}NO_2sal)pn)]_2$ is the only member of the series to have the Mn ions related though an inversion center. The molecule has bond lengths consistent with the trivalent oxidation state and has a Jahn−Teller elongation along the O2−Mn1−O3 bonds. This axial elongation is accompanied by the compression of the other Mn^{III}−ligand bond lengths. This fact coupled with the orientation of the Jahn−Teller axis symmetrically through the bridging alkoxo atoms causes this compound to have the shortest Mn···Mn distance of the series: 3.24 Å. It is interesting to compare this complex with the asymmetric monoalkoxide-bridged dimer that was previously reported.[20] The long Mn1−O2 bond (2.331 Å) is similar to that observed for the Jahn−Teller-distorted Mn−alkoxide bond found for $[Mn^{III}_2(2\text{-}OH(5\text{-}Cl\text{-}sal)pn)_2(MeOH)]$·MeOH, **5** (2.35 Å). Of course, in the case of the asymmetric dimer, the lack of a second bridging ligand allows the Mn−O−Mn angle to increase to 128.9° vs 99.1° for the symmetrically bridged dimer. This allows the Mn−Mn separation in **5** to increase to 3.81 Å.

The most highly oxidized dimer in the series, $[Mn^{III}Mn^{IV}(2\text{-}OH(3,5\text{-}Cl_2sal)pn)_2](ClO_4)$, **4**, is composed of valence-localized Mn ions, both in the solid state and in solution (*vide infra*). The Mn^{IV} ion has common Mn^{IV}−ligand bond lengths. The Mn^{III} ion is characterized as the first example in manganese complexes of a pseudo-C_{2v} Jahn−Teller distortion. The two alkoxide−Mn bonds are 0.27 and 0.35 Å longer than the two phenolate−Mn bonds. This configuration is presumably dominated by the electron-deficient Mn^{IV} having strong metal−ligand bonds. This unusual orientation and therefore small metal−ligand−metal orbital overlap lead to very weak exchange between metal atoms (*vide infra*) and the longest Mn···Mn distance known for a $Mn^{III}Mn^{IV}$ dimer bridged by two atoms. Previously the structure of the monoalkoxide-bridged dimer $[Mn^{III}Mn^{IV}(2\text{-}OH(3,5\text{-}Cl_2sal)pn)_2(THF)](ClO_4)$, **6**, was reported.[22] This complex was characterized by an axial elongation of the Mn^{III}−alkoxide bond trans to an exogenous THF ligand and a Mn−Mn separation of 3.65 Å. This Jahn−Teller axis

has bond lengths very similar to those observed for the bridging alkoxide−Mn^{III} bonds found in **4a**.

Redox Properties of the Dimers. The electrochemistry of the complex with the 5-NO_2 derivative of the ligand (the most electron-withdrawing group) shows that all four oxidation states can be obtained using the same ligand (Figure 4). This was confirmed by the preparation and isolation of all four dimers for the 5-Cl ligand set. We prepared the various derivatives for solubility and crystallization properties. As is indicated from the cyclic voltammogram in Figure 4, even as the 5-NO_2 derivative, the Mn^{II}_2 dimer is not stable to air oxidation. However, all of the derivatives can be handled in air for some time as dry powders or crystals.

The electrochemical responses of the other substituted-ring derivatives were measured, and the results are compiled in Table 3. The III/IV ↔ III_2 and III_2 ↔ III/II couples are shown for each of the five substituted-ring dimers: 5-MeO, 5-H, 5-Cl, 3,5-Cl_2, and 5-NO_2. The difference between the III/IV ↔ III_2 and III_2 ↔ III/II redox couple for the series only varies by 13 mV (570−583 mV). On the basis of these values, a comproportionation constant can be calculated for the Mn^{III}_2 species, where $\log K_{com} = \Delta E_{1/2}$ (V)/0.059. For this series the minimum $K_{com} = 4.6 \times 10^9$. The magnitude for this constant indicates that there is no measurable disproportionation reaction for the Mn^{III}_2 dimers in this series. The reduction potential difference between the two homovalent dimers of the 5-NO_2 ligand is 480 mV, indicating a comproportionation constant, K_{com}, of 1.4×10^8. This value is somewhat smaller than that measured for the Mn^{III}_2 dimer. This suggests that disproportionation is small but more likely for the mixed-valent dimers than for the homovalent complexes. The $Mn^{II}Mn^{III}$ dimers of both the 5-Cl and the 3,5-Cl_2 ligands are nearly insoluble in acetonitrile, so it is probable that this insolubility helps to drive the comproportionation reaction to completion. It was probable that the earlier reports[22] of the asymmetric derivatives of these complexes showing reversible oxidation from the Mn^{III}_2 to the $Mn^{III}Mn^{IV}$ complex in acetonitrile had the symmetric dimer as the primary species in solution.

EPR Spectroscopy. As shown in Figure 5, three of the four oxidation states for this dimer series are EPR active. The EPR spectrum of the Mn^{II}_2 dimer is characteristic of weakly coupled Mn^{II} ions. The spectrum for $Na_2[Mn^{II}_2(2\text{-}OH(5\text{-}NO_2sal)pn)_2]$ is shown at 5 K. This spectrum is very similar to those observed for the fully reduced form of the Mn catalase from *T. thermophilus*.[4] While most other Mn^{II} dimers are EPR silent at 5 K due to the $S = 0$ ground state, this complex has similar spectra at both low temperature and 77 K. This is consistent with the ferromagnetic coupling observed for this complex. While hyperfine splittings due to electronic interaction with two $S = {}^5/_2$ Mn nuclei usually dominate the EPR spectra of dimeric manganese(II) complexes and proteins, the hyperfine lines are rather weak for this dimer. The splittings can be observed on the features at ∼1100 and ∼2600 G. The hyperfine splittings for these dimers average 46 G, consistent with the effect of electronic interaction with two coupled Mn^{II} ions.

The EPR spectrum observed for the $Mn^{II}Mn^{III}$ dimer is also consistent with ferromagnetic coupling in the solid state. Most $Mn^{II}Mn^{III}$ dimers that have been reported exhibit features at $g = 5-7$ at 77 K, and upon lowering of the temperature, a $g = 2$ multiline signal dominates.[38−40] This signal is consistent with weak antiferromagnetic coupling between the Mn ions. The range of reported exchange parameters for structurally characterized $Mn^{II}Mn^{III}$ dimers is from −1 to −7.7 cm^{-1}. The (TEA)-$[Mn^{II}Mn^{III}(2\text{-}OH(5\text{-}Cl\text{-}sal)pn)_2]$ system has a $g = 7$ absorptive feature at 77 K. This signal becomes more intense upon lowering the temperature to 5 K but remains at the same field in the spectrum. This is due to the $S = {}^9/_2$ ground state for this complex. The spectrum shown in Figure 5B is consistent with and nearly identical to the powder spectrum of the only other reported ferromagnetically coupled $Mn^{II}Mn^{III}$ dimer.[34]

Magnetism. Previously we[20,22] and others[21] examined the magnetic interactions of the asymmetric Mn^{III}_2 and $Mn^{III}Mn^{IV}$ dimers, and the exchange parameter J was found to be very low, −3.55 cm^{-1} for $[Mn^{III}_2(2\text{-}OH(5\text{-}Cl\text{-}sal)pn)_2(MeOH)]\cdot$ MeOH, **5**, and −10 cm^{-1} for $[Mn^{III}Mn^{IV}(2\text{-}OH(3,5\text{-}Cl_2sal)pn)_2\text{-}(THF)](ClO_4)$, **6**. In this work, we present the first magnetostructural study of a dimer system in four different oxidation states having an invariant ligand set. Table 4 compiles the magnetic parameters of the symmetric and asymmetric dimers of the 2-OHsalpn ligand. One might anticipate that the symmetric dimers would exhibit stronger exchange coupling than the asymmetric dimers since there is a shortening of the Mn−Mn separation and a second alkoxide bridge is inserted between the metal ions. However, the exchange parameters compiled in Table 4 show that these compounds are slightly less strongly coupled. This apparent change in coupling between the metal atoms may be due to the tightening of the Mn−O−Mn bond angle with the second exchange pathway in place. Smaller Mn−O−Mn bond angles leading to accidental orthogonality of the magnetic orbitals (90° pathways) would be expected to increase the ferromagnetic contributions to the exchange coupling parameter, J.[41−43]

In 1991, Gorun and Lippard developed a magnetostructural correlation for magnetically coupled iron(III) dimers.[44] In that work, they examined a series of binuclear Fe^{III} complexes containing at least one oxo atom (oxo, hydroxo, alkoxo) bridge that had been characterized by crystallography and by magnetic susceptibility studies and correlated the magnetic exchange interaction to a structural parameter. While previous studies involving Cu and Cr complexes indicated that the magnetic exchange coupling is related to structural features such as the M−O−M angle and the M−O bond length,[45,46] no analogous relationship had been developed for iron or manganese. Lippard's study showed that the bridging angle may be important for similar complexes but that no general trend could be developed. Gorun and Lippard introduced a parameter P for their correlation which is defined as the average of the shortest distance between the metal atoms and the bridging atom. As P decreased, the exchange coupling increased; a general trend of increasing metal−metal distance is also correlated to decreased magnetic exchange.[44]

This type of relationship is consistent with qualitative observations for Mn complexes as well, with strongly coupled high-valent dioxo-bridged dimers having very short Mn−Mn distances and the low-valent alkoxide- and phenoxide-bridged dimers characterized by weak exchange. There are not nearly the number of structurally and magnetically characterized Mn dimers as there are for either iron or copper, and a detailed

(38) Diril, H.; Chang, H.-R.; Nilges, M. J.; Zhang, X.; Potenza, J. A.; Schugar, H. J.; Isied, S. S.; Hendrickson, D. N. *J. Am. Chem. Soc.* **1989**, *111*, 5102−5114.
(39) Buchanan, R. M.; Oberhausen, K. J.; Richardson, J. F. *Inorg. Chem.* **1988**, *27*, 971.
(40) Chang, H.-R.; Larsen, S.; Pierpont, C. G.; Boyd, P. D. W.; Hendrickson, D. N. *J. Am. Chem. Soc.* **1988**, *110*, 4565.
(41) Hatfield, W. E. In *Theory an Applications of Molecular Paramagnetism*; Boudreaux, E. A., Mulay, L. N., Eds.: John Wiley and Sons: New York, 1976; pp 349−450.
(42) Kahn, O. *Angew. Chem., Int. Ed. Engl.* **1985**, *24*, 843.
(43) Hay, P. J.; Thibeault, J. C.; Hoffmann, R. *J. Am. Chem. Soc.* **1975**, *97*, 4884.
(44) Gorun, S. M.; Lippard, S. J. *Inorg. Chem.* **1991**, *30*, 1625−1630.
(45) Willett, R. D. In *Mangeto-Structural Correlations in Exchange Coupled Systems*; Willett, R. D., Gatteschi, D., Khan, O., Eds.; D. Reidel: Dordrecht, The Netherlands, 1985; pp 389−420.
(46) Hatfield, W. E. *Comments Inorg. Chem.* **1981**, *1*, 105.

correlation has not been made. Interestingly, the superexchange pathway for this set of dimers, **1a**−**4**, defined as *P* only ranges from 2.155 to 2.063 Å. The values of *P* for the Mn^{III}_2 and $Mn^{III}Mn^{IV}$ dimers are nearly identical for both the symmetrically bridged dimers and the asymmetric monoalkoxide-bridged dimers, which may explain the similar magnitudes of *J* observed between these structurally dissimilar systems.

A study using the strongly coupled Mn^{IV} dimer $[Mn^{IV}(salpn)(O)]_2$ showed that protonation of the oxo bridges causes a dramatic decrease in the exchange coupling between the Mn ions.[47] The antiferromagnetic exchange coupling decreased from -92 cm^{-1} for the dioxo-bridged dimer, to -48 cm^{-1} for the monoprotonated bridged complex, to -6 cm^{-1} for the diprotonated dimer. Alkoxide oxygens are similar to hydroxide bridges in the arrangement of the p orbitals available for overlap with metal orbitals as potential exchange pathways. That is, alkoxide bridges would be expected to be poor exchange pathways between manganese ions, precisely what is observed in these complexes.

The net exchange interaction in dimeric systems containing the d^4 Mn^{III} ion or the d^5 Mn^{II} ion is expected to be a combination of ferromagnetic and antiferromagnetic contributions.[38,41−43] The smaller bridge angle resulting from the second bridge present in these symmetric dimers can be contributing to the ferromagnetic exchange between the Mn ions. For the low-valent dimers $(TMA)_2[Mn^{II}_2(2\text{-}OH(5\text{-}NO_2sal)pn)_2]$, **1b**, and $(TEA)[Mn^{II}Mn^{III}(2\text{-}OH(5\text{-}Cl\text{-}sal)pn)_2]$, **3a**, net ferromagnetic coupling is observed. In the case of $[Mn^{III}_2(2\text{-}OH(5\text{-}Cl\text{-}sal)pn)_2]$, **2**, and $[Mn^{III}Mn^{IV}(2\text{-}OH(3,5\text{-}Cl_2sal)pn)_2](ClO_4)$, **4**, additional ferromagnetic pathways lower the net antiferromagnetic exchange coupling and give low values of *J* versus those observed for the asymmetric derivatives. For example, the coupling between the Mn ions in **4** is only -2 cm^{-1} versus -10 cm^{-1} for the asymmetric complex $[Mn^{III}Mn^{IV}(2\text{-}OH(3,5\text{-}Cl_2sal)pn)_2(THF)](ClO_4)$, **6**.

One may also attempt to understand the relative sign and magnitude of the exchange interactions in these complexes by comparing the experimentally determined *J* values with the electronic structure (d orbital occupancy) of the constituent Mn ions, paying close attention the orientation of the Jahn−Teller axis on Mn^{III}. It should be re-emphasized at this point that all of the exchange interactions in this dimer series are weak, and the behavior of the χ vs *T* data clearly determine the sign of the exchange interaction, while the fits to the data quantify the magnitude of the exchange interaction. For $(TMA)_2[Mn^{II}_2(2\text{-}OH(5\text{-}NO_2sal)pn)_2]$, the Mn^{II}_2 ions are d^5 high spin and all of the d orbitals are magnetic orbitals with the e_g σ-bonding set having a greater pathway-dependent contribution to the measured exchange interaction, *J*, than the t_{2g} π-bonding orbitals. In this case, the in-plane $d_{x^2-y^2}$ orbitals would be expected to dominate the exchange due to orbital directionality and M−L overlap considerations. However, the tight 101.4° bridge bond angle probably leads to accidental orbital orthoganality,[41−43] resulting in a net small measured ferromagnetic exchange interaction. In the case of $(TEA)[Mn^{II}Mn^{III}(2\text{-}OH(5\text{-}Cl\text{-}sal)pn)_2]$, the Mn^{III} Jahn−Teller axis is best defined as a d_{z^2} compression along O6−Mn1−O5. This places the single e_g electron in a σ-bonding $d_{x^2-y^2}$ orbital which is perpendicular to the O6−Mn1−O5 vector. This unusual axial compression results in the complex possessing the longest Mn···Mn distance in the dimer series. A complex combination of potentially orthogonal d−d interactions between the Mn^{III} $d_{x^2-y^2}$ orbital and the in-plane orbitals of Mn^{II}, coupled with the long Mn···Mn distance, results in weak ferromagnetic exchange in $(TEA)[Mn^{II}Mn^{III}(2\text{-}OH(5\text{-}Cl\text{-}sal)pn)_2]$. The third member of the dimer series, $[Mn^{III}(2\text{-}OH(5\text{-}NO_2sal)pn)]_2$, possesses the largest exchange interaction in the series, which was determined to be antiferromagnetic in nature. In this dimer, the individual Mn^{III} ions are elongated along the O2−Mn1−O3 bonds. Furthermore, the halves of the dimer are related by inversion symmetry. The combination of the inversion symmetry and in-plane axial elongation results in a shortest Mn···Mn distance in the series. The presence of inversion symmetry results in nonorthogonal d_i−d_i ($i = xy, xz, yz, x^2 - y^2, z^2$) interactions between the two dimers. This fact, coupled with the shorter Mn···Mn distance, increases the antiferromagnetic contributions to the exchange. Finally, we consider the mixed-valent dimer $[Mn^{III}Mn^{IV}(2\text{-}OH(3,5\text{-}Cl_2sal)pn)_2(THF)](ClO_4)$. The Mn^{IV} ion may be said to display effective O_h symmetry, and the d^3 ion has only the t_{2g} π-bonding orbitals singly occupied. This is in stark contrast to the unusual C_{2v} Jahn−Teller distortion found at the Mn^{III} site. As a result, ineffective t_{2g}−t_{2g} π-pathways must dominate the exchange. This fact, coupled with the presence of a nonoxo bridging ligand, results in a poor superexchange pathway, and the complex displays weak antiferromagnetic coupling. This is the first series that allows the observation of the effect of subtle changes in geometry on the sign if not the magnitude of magnetic exchange in dimeric systems across a range of oxidation states. The modulated effect of these exchange pathways in the presence of strongly coupled nuclei in larger Mn systems (e.g., tetranuclear clusters) may well be present but, due to the magnitude of coupling, is not observed in these systems.

Summary

This report provides the first dinuclear Mn series spanning four oxidation states utilizing an invariant ligand set that has been characterized crystallographically. The $[Mn_2(2\text{-}OH(Xsal)pn)_2]$ series has been isolated and characterized in each of the four known oxidation states observed for the Mn catalases. This detailed study of the structural, spectroscopic, and magnetic properties of these complexes and comparison to the monoalkoxide-bridged complexes previously reported show the versatility achievable with dimeric complexes of these ligands. Furthermore, the similarities of the various oxidation state dimers may give insight into the wide-ranging reaction chemistry observed for these complexes.[11,24,48] These complexes can also act as a functional mimic for the reactivity and inactivation of the Mn catalases.[11] The chemistry of these reactions and the accompanying spectroscopy will be discussed separately.[24]

Acknowledgment. This work was funded by National Institutes of Health Grant GM 39020 to V.L.P. and National Science Foundation Grant CHE9316557 to M.L.K.

Supporting Information Available: Tables containing complete crystallographic experimental details, positional parameters, thermal parameters, bond lengths, and bond angles as well as ORTEP diagrams with complete numbering schemes for **1a**, **3a**, and **4a** and a figure showing UV−visible spectra for the four $[Mn_2(2\text{-}OH(5\text{-}Cl\text{-}sal)pn)_2]$ dimers (56 pages). Ordering information is given on any current masthead page.

IC970140I

(47) Baldwin, M. J.; Stemmler, T. L.; Riggs-Gelasco, P. J.; Kirk, M. L.; Penner-Hahn, J. E.; Pecoraro, V. L. *J. Am. Chem. Soc.* **1994**, *116*, 11349−11356.

(48) Caudle, M. T.; Riggs-Gelasco, P.; Gelasco, A. K.; Penner-Hahn, J. E.; Pecoraro, V. L. *Inorg. Chem.* **1996**, *35*, 3577.